Progress in Oceanography 219 (2023) 103161

Contents lists available at ScienceDirect

Progress in Oceanography

journal homepage: www.elsevier.com/locate/pocean

Diffusive and advective cross-frontal fluxes of inorganic nutrients and dissolved inorganic carbon in the Barents Sea in autumn

Zoe Koenig [a,b,c,*], Ilker Fer [b], Melissa Chierici [d], Agneta Fransson [a], Elizabeth Jones [d], Eivind H. Kolås [b]

[a] Norwegian Polar Institute, Tromsø, Norway
[b] Geophysical Institute and Bjerknes Center for Climate Research, University of Bergen, Bergen, Norway
[c] UiT The Arctic University of Norway, Tromsø, Norway
[d] Institute of Marine Research, Tromsø, Norway

ARTICLE INFO

Keywords:
Nutrient fluxes
Barents Sea
Polar front

ABSTRACT

The Atlantic Water, entering the Arctic through the Barents Sea and Fram Strait, is the main source of nutrients in the Arctic Ocean. The Barents Sea is divided by the Polar Front into an Atlantic-dominated domain in the south, and an Arctic-dominated domain in the north. The Polar Front is a thermohaline structure, which is topographically-steered at sub-surface, and influenced by the seasonal sea ice edge near the surface. Exchanges of nutrients between the inflowing Atlantic Water and the surrounding waters are key for the primary production in the Barents Sea. In October 2020, we measured nutrients (nitrate, phosphate and silicic acid), dissolved inorganic carbon (DIC), ocean stratification, currents and turbulence in the vicinity of the Polar Front in the Barents Sea within the framework of the Nansen Legacy project, allowing estimates of horizontal and vertical advective fluxes and turbulent fluxes of nitrate and DIC. We studied the autumn situation when primary production was declining. We found a substantial transfer of nitrate and DIC across the Polar Front from the Atlantic domain to the Arctic domain. Up to one quarter of the replenishment of the nitrate in the mixed layer during winter could be attributed to vertical mixing during wind events, shared approximately equally between advective and turbulent fluxes. The vertical turbulent fluxes bring nutrients from the subsurface Atlantic Water to the surface. We also identified an export of nitrate and DIC from the Barents Sea to the Nordic Seas occurring along the eastern shelf of Svalbard. Our study shows the role of vertical fluxes in fall and winter to precondition for the following spring bloom.

1. Introduction

The Barents Sea and eastern Fram Strait are gateways of Atlantic Water inflow into the Arctic Ocean (Fig. 1). The Atlantic Water is an important source of heat, salt, dissolved inorganic carbon (DIC) and nutrients in the Arctic. Torres-Valdés et al. (2013) found that one of the major net source of nutrients in the Atlantic-influenced Arctic is the inflow through the Barents Sea Opening (34 kmol s^{-1}, which represents about 37% of the total import into the Arctic).

Atlantic Water flows through the Barents Sea and enters the Arctic Ocean through the St Anna Trough (Schauer et al., 2002). The circulation in the Barents Sea is complex with several branches of Atlantic Water circulating around different banks of the Barents Sea (Ingvaldsen et al., 2002; Loeng, 1991). Complexity is added to this general circulation by relatively strong tidal currents and eddies that add significant variability (Våge et al., 2014). The Barents Sea is divided into an Atlantic-dominated domain in the south and an Arctic-dominated domain in the north. Those two regions are separated by the polar front, typically located along the 200 m isobath (Oziel et al., 2016; Barton et al., 2018). The location of the front in the upper 50 m of the water is influenced by the sea ice edge, while the sub-surface front is relatively stationary, but varies with tides and eddies.

With ongoing climate change and Atlantification of the Barents Sea (Årthun et al., 2012) and more generally of the Arctic Ocean (Polyakov et al., 2017), the Barents Sea is warming (Smedsrud et al., 2013; Skagseth et al., 2020) and is already largely ice-free in summer (Onarheim et al., 2018). This has implications for the stratification and the supply of nutrients into the surface layers, primary production and the marine ecosystems in the Arctic Ocean and in the Barents Sea (Ingvaldsen et al., 2021). For example, recent increases in Atlantic Water transport through the Barents Sea have resulted in an increased supply of nutrients, which could explain the observed increase in primary production and concentrations of chlorophyll a (Lewis et al., 2020).

* Correspondence to: University of Tromsø, Tromsø, Norway.
E-mail address: zoe.c.koenig@uit.no (Z. Koenig).

https://doi.org/10.1016/j.pocean.2023.103161

Available online 4 November 2023

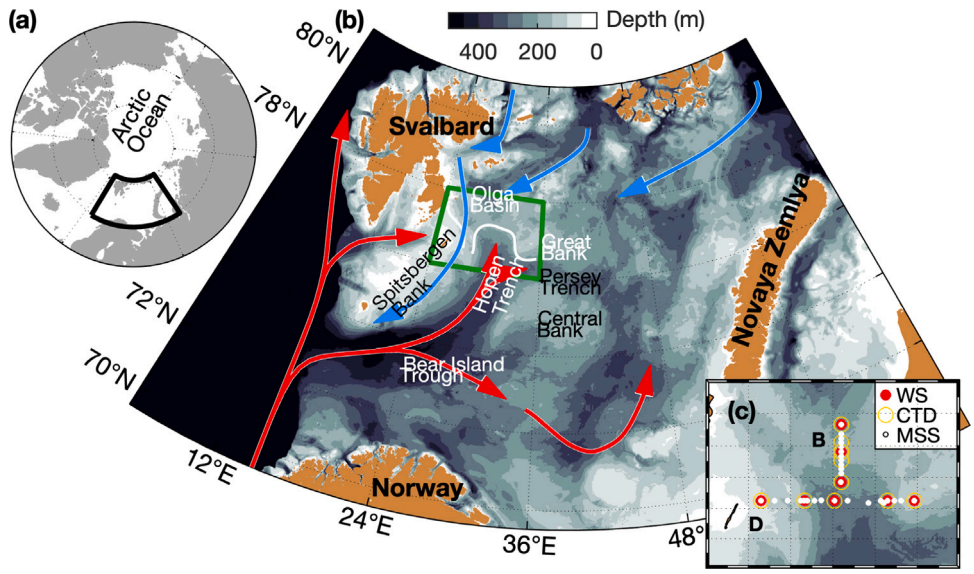

Fig. 1. (a) Arctic map with the Barents Sea shown by the black box. (b) Atlantic Water inflow and polar water circulation in the Barents Sea. The red lines illustrate the Atlantic Water branches, the blue arrow is the Polar Water branches. The white line highlights the location of the Polar Front. Background is the bathymetry. The green box is the study region shown in panel c. (c) Close-up of the sampling in sections B and D. WS: Water sampling, CTD: Conductivity–Temperature–Depth profiles, and MSS: Microstructure profiles. Bathymetry is from IBCAO-v4 (Jakobsson et al., 2012).

Biological processes play a major role in the Arctic carbon cycle and the oceanic CO_2 uptake of atmospheric CO_2 (Chierici et al., 2011, 2018). High pH and low partial pressure of CO_2 (pCO_2) in surface waters in spring and summer are mainly due to CO_2 uptake by primary producers during the growing season (Chierici et al., 2018; Jones et al., 2021). About 70% of the total CO_2 uptake in the Barents Sea is a result of biological CO_2 uptake (Fransson et al., 2001). Since the surface waters beneath sea ice are typically under-saturated in CO_2 relative to the atmospheric levels, increased areas of open water can lead to enhanced ocean uptake of atmospheric CO_2, particularly in combination with strong winds that increase the potential of oceanic CO_2 uptake, i.e. a sink for atmospheric CO_2 (Fransson et al., 2017). Storm events and ice-free, open water also promote vertical mixing and reduce stratification of the water column (Graham et al., 2019; Meyer et al., 2017). With weaker stratification in the northern Barents Sea (Lind et al., 2018), leading to increased exchange of heat and gas between the ocean and atmosphere (Fer, 2009), substantial changes can be expected in CO_2 sink capacity of the ocean when combined with reduced sea-ice cover.

Studies north of Svalbard suggest that the relative impact of the seasonal supply of nutrients resulting from winter convection is the most important process in providing nitrate compared to turbulence-induced nutrient fluxes (Randelhoff et al., 2016). However, such analysis has not been performed in the Barents Sea. In this study, we investigated the exchanges between the Atlantic Water and the surrounding water masses in the vicinity of the Polar Front in the northwestern Barents Sea. We computed the vertical and horizontal fluxes of inorganic nutrients and carbon. The goal was to quantify the exchanges between the Arctic domain and the Atlantic domain of the Barents Sea (advection and horizontal fluxes), and between the Atlantic water and the mixed layer (vertical fluxes). The latter controls the transport of nutrients to the upper water column layer where all the primary production is taking place. In Section 2 we describe the data used in this study and how the advective and diffusive fluxes of nitrate and dissolved inorganic carbon are computed; these estimates are then presented in Section 3 and discussed in Section 4. Finally, we summarize our results in Section 5.

2. Data and methods

Data were collected during a cruise (GOS 2020113) onboard the Norwegian research vessel G.O. Sars (October 6–October 27, 2020) within the framework of the Nansen Legacy project (Fer et al., 2021). We present here two main hydrographic sections that were occupied during the cruise in autumn (Fig. 1). Section B crosses a bathymetric sill in the Barents Sea (along longitude 30.5°E), where the Polar Front is located (Fig. 1). This section was repeated five times, but water samples were taken only during the first occupation (hereafter B_{1R}, from 14 October 2020 12:15 to 15 October 2020 00:05, all times are given in the Coordinated Universal Time), and the fifth repeat (hereafter B_{2R}, from 17 October 2020 18:30 to 18 October 2020 02:40). The two repeat sections are separated by 3 days. A second section, section D, was carried out on 19 October 2020, along latitude 76.75°N, south of the polar front, crossing two slopes where the Atlantic water flows (Fig. 1).

2.1. Hydrographic and chemistry data

Water column hydrography was investigated using vertical profiles of temperature and salinity obtained with a conductivity–temperature–depth (CTD, SBE-911 plus) sensor mounted on a rosette equipped with 24-Niskin bottles used for seawater sampling. The CTD was equipped with additional sensors for chlorophyll a fluorescence (Chlfluo) (Chelsea Aqua 3) and dissolved oxygen (DO). Pressure, temperature, and practical salinity data from the CTD are accurate to ±0.5 dbar, $\pm 10^{-3}$ °C, and $\pm 3 \times 10^{-3}$, respectively. CTD data were processed using the standard SBE Data Processing software. Salinity measurements were corrected against water samples that were analyzed using a Guildline Portasal 8410 salinometer. The biogeochemical sensors were calibrated against values derived from water samples using, for chlorophyll a, spectrophotometric (Turner designs, see the sampling protocol: The Nansen Legacy (2021)) and for DO the Winkler titration method as described in the cruise report (Fer et al., 2021). CTD measurements from the ship are available from Fer et al. (2023b).

Water column dissolved inorganic carbon (DIC) and inorganic nutrients (nitrate [NO_3^-], nitrite [NO_2^-], phosphate [PO_4^{3-}], and silicic acid [$Si(OH)_4$]) were investigated from water samples collected from the CTD-Rosette system at each station for the whole water column. Nutrient samples were sampled into 20 mL vials, preserved with 250 μL chloroform and stored dark at 4 °C. Post-cruise analyses were performed using a colorimetric method (Grasshoff, 1983; Gundersen et al., 2022) at the Institute of Marine Research, Bergen, Norway. The detection limits were 0.5 mmol m^{-3} for [NO_3^-], 0.06 mmol m^{-3} for

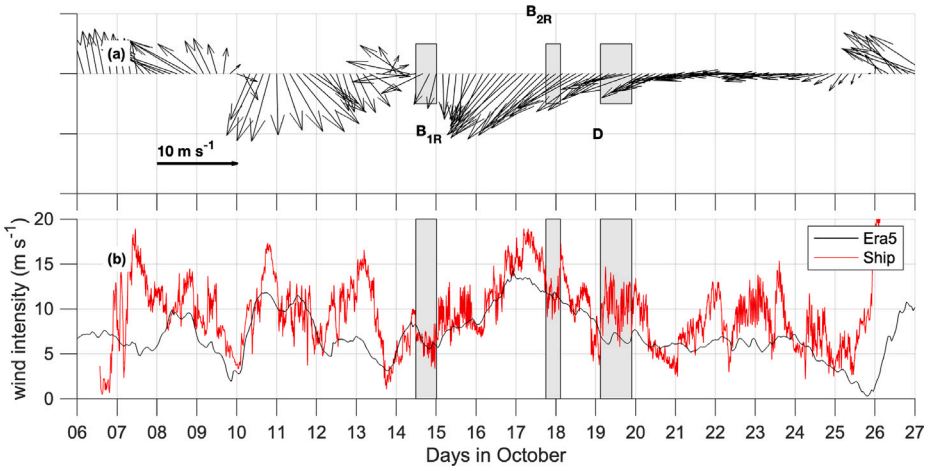

Fig. 2. (a) Wind arrows and (b) wind intensity (in m s^{-1}) at 77°N, 30°E from ERA5 (black) during the cruise. Wind intensity from the ship's weather mast at 25 m height along the ship trajectory is shown in red. The gray rectangles indicate the duration of hydrographic sections. B_{1R} /B_{2R}: First/Second repeat of the B transect respectively, and D: section D.

[PO_4^{3-}] and 0.7 mmol m^{-3} for [$Si(OH)_4$], respectively. The [NO_2^-] concentrations were very low and near zero, thus [NO_3^-] refers to the sum of nitrite [NO_2^-] and nitrate [NO_3^-].

Samples for DIC were stored cool and dark in 250 ml borosilicate samples, preserved with 50 µL saturated mercuric chloride solution and were analyzed by coulometric titration of extracted acidified sample (Johnson et al., 1999) using a Versatile Instrument for the Determination of Titration carbonate (VINDTA 3D, Marianda, Germany). The DIC measurements were checked against certified reference material (CRM, provided by A. G. Dickson, Scripps Institution of Oceanography, USA, Dickson et al. (2007)) and precision and accuracy were determined from triplicate in-bottle analyses as ±2 µmol kg^{-1}.

We use the Apparent Oxygen Utilization (AOU), defined as AOU = $[O_2]_s - [O_2]$ where $[O_2]_s$ is the oxygen saturation of the dissolved oxygen (DO) at the temperature (T), salinity (S) and pressure (P) of the water, and $[O_2]$ is the measured oxygen concentration (DO). Positive AOU represents oxygen utilization through respiration and negative AOU refers to oxygen production through photosynthesis.

2.2. Current data

The CTD frame was fitted with a pair of acoustic Doppler current profilers (ADCPs), so-called lowered-ADCPs (LADCPs). The LADCPs were 6000 m-rated 300 kHz Teledyne RD Instruments (RDI) Sentinel Workhorses, one mounted pointing downward and one upward. The LADCPs were synchronized and set to provide data vertically averaged in 8 m bins. Compasses were calibrated on land prior to cruises with resulting errors less than 1–2°. LADCP data were processed using the LDEO software version IX-13 based on Visbeck (2002). The LADCP profiles were constrained by navigation data and 5-min averaged profiles from the ship's hull-mounted ADCP (SADCP, 75 kHz). Ocean current measurements from the ship are available from Fer et al. (2023b).

The detided version of the LADCP data was obtained by subtracting the barotropic tidal currents from the observations. Barotropic tidal currents were obtained from the Arctic Ocean Inverse Tide Model on a 5 km horizontal grid (Arc5km2018) (Erofeeva and Egbert, 2020). We used the 8 main constituents (M_2, S_2, N_2, K_2, K_1, O_1, P_1, Q_1) and 4 nonlinear components (M_4, MS_4, MN_2, and $2N_2$), to predict the horizontal tidal volume transport (m^2 s^{-1}) at profile location and time, and obtain the currents by dividing by the local depth.

2.3. Microstructure profiler data

The turbulence data were collected using a loosely tethered free-fall MSS-90L microstructure profiler (Prandke and Stips, 1998) developed by ISW Wasser-messtechnik, Germany. The profiler had precision conductivity, temperature, and pressure sensors as well as microstructure sensors including two airfoil shear probes, a fast response thermistor, and a micro conductivity sensor, all sampling at 1024 Hz. Data processing follows the recommendations and conventions of the SCOR Working Group on analyzing ocean turbulence observations to quantify mixing (ATOMIX, http://wiki.uib.no/atomix), see also Fer et al. (2022). Final processed profiles include 0.1 m vertically averaged temperature and salinity, and 2–2.5 m vertical resolution turbulent dissipation rate estimates. Reported accuracies of the sensors by the manufacturer were 0.1 m, 0.0028 °C, and 0.003 mS cm^{-1} for depth, temperature, and conductivity, respectively. Using profiles paired with the shipboard CTD that is already calibrated against water samples, we apply an offset correction to the salinity measured by the MSS. The estimated accuracy in the MSS salinity measurements is 0.01 on the practical salinity scale.

The dissipation rate of turbulent kinetic energy per unit mass, ϵ, is estimated using the isotropic relation and by integrating the turbulent shear spectra. Shear spectra are calculated using record lengths of 6 s (sliding by 3 s) and FFT lengths of 2 s (50% overlapped). Vibration-coherent noise is removed using the method of Goodman et al. (2006). Resulting values were quality-screened following the recommendations of ATOMIX. A final dissipation rate estimate is obtained by averaging the estimates from the two probes when they agree within 95% confidence intervals (Lueck, 2022), or the minimum estimate if they do not. The noise level of the dissipation rate measured by the MSS is about $(1-3)\times10^{-9}$ W kg^{-1}. Dissipation measurements from the upper 10 m were excluded because of the disturbance from the ship's keel, and the profiler's adjustment to free fall. Ocean microstructure measurements from the ship are available from Fer et al. (2023a), including all ATOMIX levels from the full resolution time series to dissipation estimates, together with their associated wavenumber spectra.

2.4. Wind data

Wind data are from the reanalysis product ERA5 (Hersbach et al., 2018). We use the 6-hour-average wind speeds at 10 m height. In this analysis, time series of wind speeds were extracted at 77°N, 30°E (Fig. 2). ERA5 winds compare well with the measurements from the ship's weather mast at 25 m height, although the ship collected data in the Barents Sea along its trajectory and was not stationary at 77°N, 30°E. This is because the atmospheric systems are large.

Wind was noticeably strong towards the south between B_{1R} and B_{2R}, with speeds reaching up to 14.5 m s^{-1} on October 17 in ERA5, and up to 18 m s^{-1} recorded by the ship. The effects of this wind event on the Polar Front dynamics are analyzed in the following sections.

2.5. Turbulent vertical fluxes

The turbulent heat flux F_H (in W m^{-2}) was calculated as :

$$F_H = -\rho_0 C_p K_\rho \frac{\partial \Theta}{\partial z} \quad (1)$$

where $\rho_0 = 1028$ kg m^{-3} is the seawater density, $C_p = 3991.9$ J kg^{-1} K^{-1} is the specific heat of seawater, Θ is the background temperature and K_ρ is the diapycnal eddy diffusivity. We thus assume that turbulence diffuses the finescale temperature gradient at the same rate as the density gradient. The sign convention is that positive heat fluxes correspond to upward heat fluxes in the water column. An upper bound for diapycnal diffusivity was obtained using the Osborn (1980) relation:

$$K_\rho = \Gamma \frac{\epsilon}{N^2} \quad (2)$$

with the mixing coefficient set to $\Gamma = 0.2$, the recommended value for the oceanic applications (Gregg et al., 2018). The buoyancy frequency or Brunt Vaisala frequency, N, was calculated using $N^2 = -\frac{g}{\rho_0}\frac{\partial \sigma_\theta}{\partial z}$, where g is the gravitational acceleration and σ_θ is the potential density anomaly referenced to surface pressure. Background vertical gradients (for temperature and density) were taken over a 10-m length scale.

Using vertical gradients between successive depths of water sampling with 25–50 m vertical separation, we obtain "coarse" turbulent fluxes of nitrate and DIC. The coarse turbulent nitrate fluxes, F_N, and the coarse turbulent fluxes of DIC, F_{DIC}, (both in μmol m^{-2} s^{-1}) are estimated as :

$$F_N = -\rho_0 \overline{K_\rho} \frac{\Delta C_N}{\Delta z} , \quad (3)$$

$$F_{DIC} = -\rho_0 \overline{K_\rho} \frac{\Delta C_{DIC}}{\Delta z} , \quad (4)$$

where C_N is the nitrate concentration and C_{DIC} is the DIC concentration. In order to be consistent with the coarse vertical spacing between the consecutive sampling depths (Δz), of nitrate and DIC concentration estimates, $\overline{K_\rho}$ is obtained by averaging K_ρ over Δz. $\frac{\Delta C}{\Delta z}$ is the discrete estimate of the gradient between two nitrate or DIC data points. Resulting estimates of nitrate and DIC fluxes are assigned to the mid-depth between two water sampling depths. Even though the nutrient sampling is coarse (from 10 to 50 m), the nutricline is resolved. When interpreting the coarse turbulent fluxes, one should bear in mind that the fluxes are averaged over 25–50 m.

In order to estimate the sensitivity of the nutrient flux computation to the coarse resolution of water samples, we use profiles of parameters resolved at high-resolution and re-calculate the turbulent fluxes at coarse resolution, using a method identical to the coarse flux calculations. We select temperature and chlorophyll-a fluorescence profiles, assuming that the vertical patchiness of chlorophyll-a could be comparable to nutrients. Additionally, we used temperature to calculate coarse heat fluxes as an alternative indicator. We calculated fluxes of chlorophyll-a and temperature at both high resolution using the average gradient over 3 m, and at coarse vertical resolution by first differencing over 25 m, using the profiles from the 49 stations where both CTD and MSS profiles were collected. Fluxes of chlorophyll-a and temperature from coarse vertical resolution calculation are then compared with the average fluxes between two water sampling depths. The root mean square of the difference between the average fluxes in the same depth-range obtained from high resolution and coarse-resolution computations varied between 60% to 200% of the average flux, depending on the depth. These discrepancies were similar for both chlorophyll-a and temperature fluxes, suggesting that we might expect a similar error in nutrient fluxes. The higher values of discrepancies were near the surface. Overall, the uncertainty is capped by a factor of two variability, which is the typical uncertainty for ocean turbulence measurements.

2.6. Advective fluxes

Horizontal advective fluxes are computed using the LADCP data at each station. We computed the horizontal advective fluxes of nitrate $A_N = (uC_N, vC_N)$ and of DIC $A_{DIC} = (u\rho C_{DIC}, v\rho C_{DIC})$ where (u, v) are the horizontal components of the velocity (from detided LADCP measurements) at the depth of the water sampling corresponding to the nitrate and DIC concentrations and ρ is the seawater density. The advective fluxes obtained at discrete depths were then averaged over three layers: 0–45 m depth which represents the mixed layer, 45–150 m depth which is the intermediate layer and 150 m to the seafloor, which is the deep layer. These boundaries were chosen after inspecting the shape of vertical profiles (see Fig. 6 for more details). One must consider that these calculations are based on detided LADCP measurements. The velocities obtained from LADCP have a margin of error of less than 3 cm/s (Thurnherr, 2010), equating to approximately 15% uncertainty in velocity intensity within this area. Some errors stem from the detiding process, especially in the dynamical region of the Polar Front in the Barents Sea. While specific error estimates for Arc5km2018 in this region are unavailable, it appears to perform reasonably well, although exact figures are not available. Consequently, we estimate errors in horizontal advective fluxes to be around 15%–20%.

Ekman pumping W_{Ek} and vertical advective fluxes of nitrate concentrations were estimated from ERA5 wind fields: $W_{Ek} = curl(\boldsymbol{\tau})/(\rho_0 f)$, with ρ_0 the seawater density, f the Coriolis coefficient and $\boldsymbol{\tau}$ the wind stress vector; $\boldsymbol{\tau} = \rho_{air} C_d \boldsymbol{u_w} |\boldsymbol{u_w}|$ where $\boldsymbol{u_w}$ is the wind speed vector at 10 m, $|\boldsymbol{u_w}|$ is the wind speed intensity at 10 m, ρ_{air} is the air density (1.25 kg m^{-3}) and $C_d = 1.25 \times 10^{-3}$ is the drag coefficient. $curl(\boldsymbol{\tau}) = \partial\tau_y/\partial x - \partial\tau_x/\partial y$. The vertical advective flux of DIC, W_{DIC}, and of nitrate, W_N, were then estimated as $W_{DIC} = \rho_0 C_{DIC} W_{Ek}$ and $W_N = \rho_0 C_N W_{Ek}$.

2.7. Water mass and layer definitions

We used the International Thermodynamic Equations of Seawater (TEOS-10) (McDougall and Barker, 2011), with Conservative Temperature (Θ) and Absolute Salinity (S_A). For this study, we follow the water mass definitions from Sundfjord et al. (2020): Atlantic Water (AW) is defined as $\Theta > 2$ °C and $S_A \geq 35.06$ g kg^{-1}, Polar Water as $\Theta \leq 0$ °C and potential density $\sigma_0 \geq 27.97$ kg m^{-3} and modified Atlantic Water as $0 < \Theta < 2$ °C and $S_A \geq 35.06$ g kg^{-1}. The Polar Front is defined as the 0 °C isotherm. The depth-latitude/longitude sections presented in Figs. 3, 4 and 5 are obtained using a Laplacian spline interpolation method with tension, choosing a 60 km search radius and no smoothing (Smith and Wessel, 1990; Pickart and Smethie, 1998). We define the pycnocline as the depth where the density exceeds 10% of the difference between the density at the surface and the density at 100 m depth. The density gradient defining the pycnocline is large, so choosing 20% of the difference instead of 10% gives similar results. The nutricline is defined as the maximum gradient in nitrate, as there are too few values on the vertical (water sampling depths) to apply the same method as for the pycnocline.

3. Results

The sections analyzed here were sampled within 5 days so the variations in nitrate concentrations and distribution could not be explained by biological activity as the main driver. We considered nitrate to be a passive tracer whose variability is predominantly affected by the ocean dynamics (e.g. advection, mixing).

3.1. Hydrographic sections

3.1.1. Section D

Section D crosses the two shelves across the Barents Sea, one shelf close to Svalbard and one shelf towards the center of the Barents Sea (Fig. 3). Both shelves have Polar Waters in the bottom layer (bottom 100 m), and are part of the Persey Current (Li and McClimans, 1998) that flows southwest. The deeper part of the basin is occupied by Atlantic Water. Nitrate, phosphate and silicic acid are concentrated in

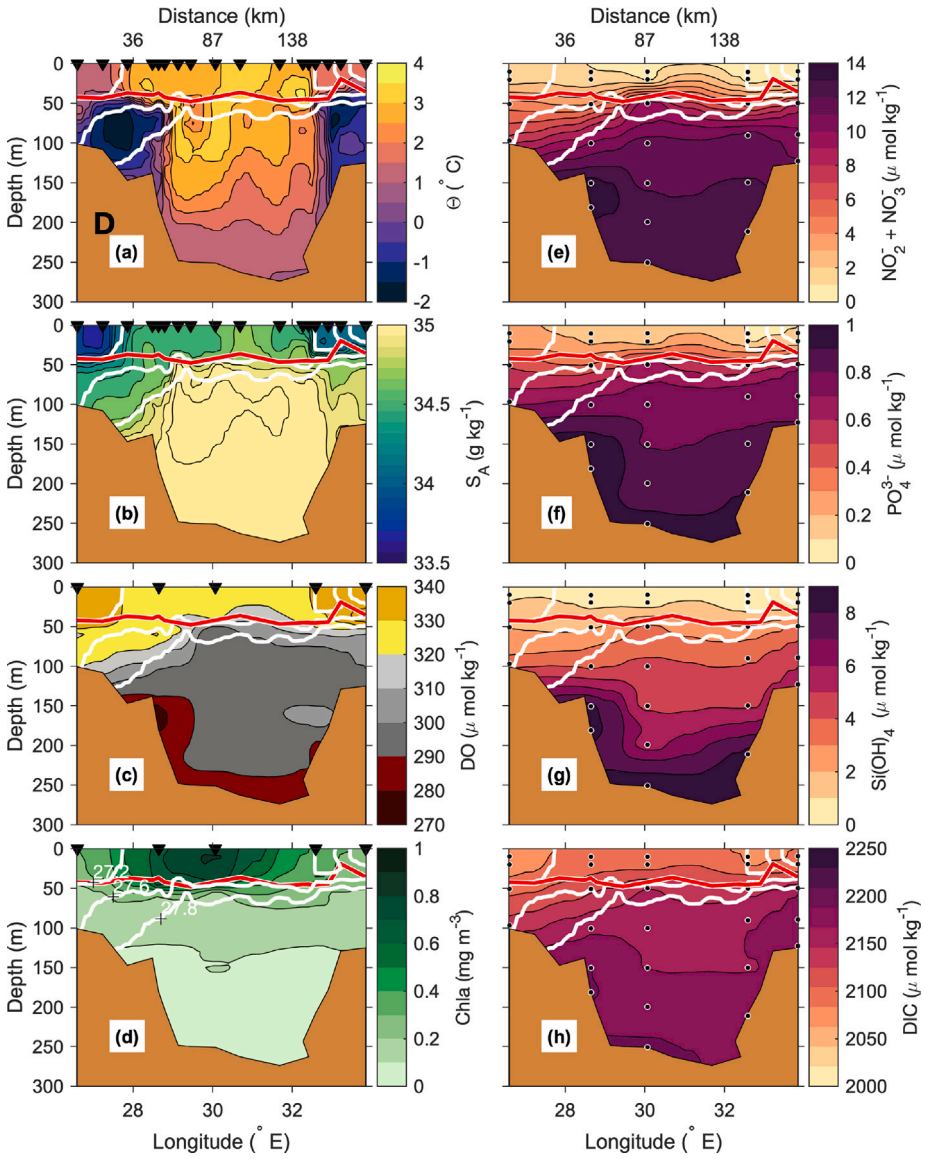

Fig. 3. Section D (a) Conservative Temperature Θ, (b) Absolute Salinity S_A, (c) Dissolved Oxygen (DO), (d) Chlorophyll a fluorescence, (e) Nitrate Concentration, (f) Phosphate Concentration, (g) Silicic Acid Concentration, (h) Dissolved Inorganic Carbon concentration. The black triangles in panels (a), (b) (c) and (d) indicate the locations of the stations (MSS for panels a and b, CTD for panels c and d). The dots in panels (e), (f) (g) and (h) indicate the water sampling locations. White lines are isopycnals obtained from the MSS profiles. Red line is the pycnocline.

the bottom layer. One distinct pattern is the higher concentration of nitrate, phosphate, DIC, silicic acid and DO at the base of the slope at about 29°E at 150 m depth, at the eastern edge of the location of the polar waters. This increase in nitrate and DIC is observed on the western slope of the section, but is absent on the eastern slope. It coincides with modified Atlantic Water flowing southwestward. After cooling and freshening in the Barents Sea, Atlantic Water recirculates along the 250 m isobath (E. Kolås personal communications), which corresponds to recirculating North Atlantic Water (Gawarkiewicz and Plueddemann, 1995). The depth of the mixed layer is constant along the section, between 45 and 50 m depth.

3.1.2. Section B

Both repeats of section B (B_{1R} and B_{2R}, Figs. 4 and 5, respectively) show the Polar Front separating the warm and salty Atlantic Water in the south from the cold and fresh Polar Waters in the north. The front in both repeats was located on the sill, slightly further south during the second repeat (from 77.3°N to 77.2°N, so about 10 km further south at 100 m depth).

The pycnocline separates surface waters that are relatively warm ($\Theta > 2$ °C) and fresh ($S_A \leq 34.4$ g kg^{-1}) from either Atlantic Water on the south side of the front or Polar Waters on the northern side of the polar front. The nutricline for nitrate is located at about 30 m depth during both transects. The pycnocline is at about 20 m/35 m during the first/second repeat of the B section respectively.

The sections of nitrate, phosphate, silicic acid and DIC concentrations show similar patterns between both repeats, with lower concentrations in the surface layer, generally increasing with depth to higher concentrations near the bottom.

In the surface layer, the apparent oxygen utilization (AOU) is close to 0 (not shown), indicating that the water is nearly saturated in dissolved oxygen (DO), and that there is no or little on-going photosynthesis. Close to the bottom the AOU reaches up to 60 μmol kg^{-1} on the northern side of the sill, indicating oxygen utilized by degradation of organic matter, releasing nutrients and DIC, and in agreement with the elevated nitrate and DIC values at the same location. This may indicate that these waters are older than those on the south side of the sill at similar depths and have not been ventilated recently. In addition,

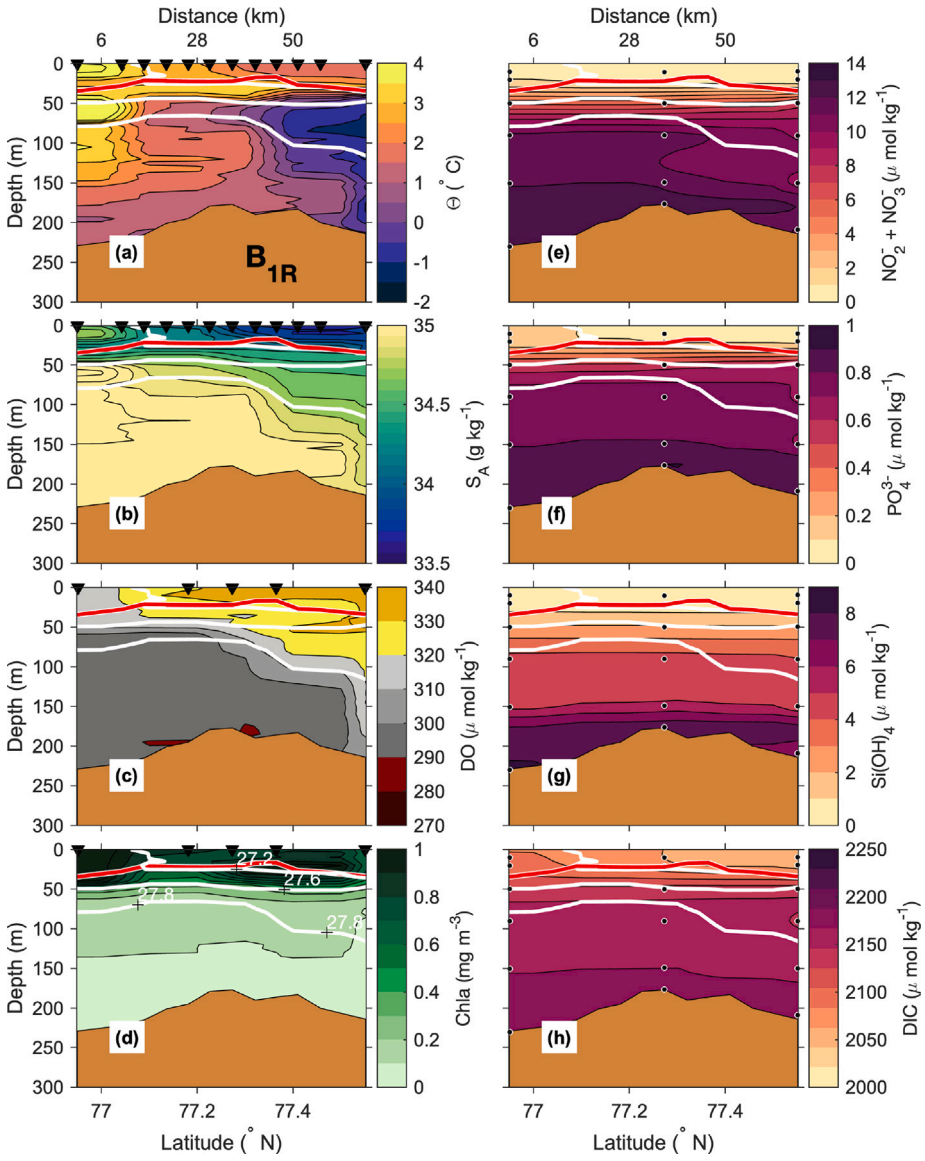

Fig. 4. Same as Fig. 3 but for the section B_{1R}: the first repeat of the B section.

these variations in the AOU, nutrients and DIC may reflect different remineralization rates and ratios in the water masses on either side of the sill. The Chlfluo reaches up to 1 mg m^{-3} in the mixed layer in B_{1R}, while it reaches only up to 0.8 mg m^{-3} during B_{2R}. These variations are significant with respect to the measurement accuracy, but could not be linked to any spatial distribution pattern as there are no ocean color satellite observations available during the cruise dates due to high cloud cover.

Some differences are noticeable between the two repeats of the section in addition to the southward shift of the location of the Polar Front. On one hand, the Polar Water at 100 m depth is found further south, and the patch of warm Atlantic Water at the southernmost stations of the section is not visible on the second repeat of the sections (Figs. 4 and 5). On the other hand, the surface layer (upper 50 m) is characterized by a steepening and a northward shift of the isopycnals and of different parameters such as nitrate and DIC.

To look further into the differences between the two repeats of the B section, Fig. 6 shows the vertical profiles of the CTD measurements with water sampling that were repeated during the two transects (one station on the northern side of the sill, one station on the sill and one station on the southern side of the sill). Interpolated profiles were obtained from fitting piecewise cubic polynomials between data points. While nitrate, phosphate and DIC profiles show a local maximum at about 40 m depth in the cold part, the silicic acid profiles do not. Variations in silicic acid in the surface layers are likely due to uptake of silicic acid by diatoms that succeeds ice algae production in this region (Reigstad et al., 2002; Assmy et al., 2017). Nitrate and phosphate reach depletion earlier in the growing season, followed by uptake of silicic acid in diatom blooms. By autumn, the water column starts to become replenished in nitrate and phosphate from subsurface waters and a shift from primary production to organic matter remineralization occurs (Henley et al., 2020; Jones et al., 2023). Silicic acid tends to be replenished later and at a slower rate, from dissolution of diatom frustules and mixing (Reigstad et al., 2002).

The Polar Waters have lower concentrations of nitrate, phosphate, silicic acid and DIC at about 150 m and at the surface, as these waters are fresher, diluted Polar Waters, while the warm Atlantic side is comparatively enriched in all nutrients (Fig. 7). Waters overlying the sill (green profiles in Fig. 6) showed the largest changes between the two repeats: the water masses encountered there are Polar Waters during B_{1R} and are Atlantic Waters during B_{2R}, suggesting a southward displacement of the front at depth. Between the first and second repeat of the transect, concentrations in the upper 20 m of nitrate, phosphate, silicic acid and DIC increased (Fig. 6a, b, c and d). Nitrate, phosphate,

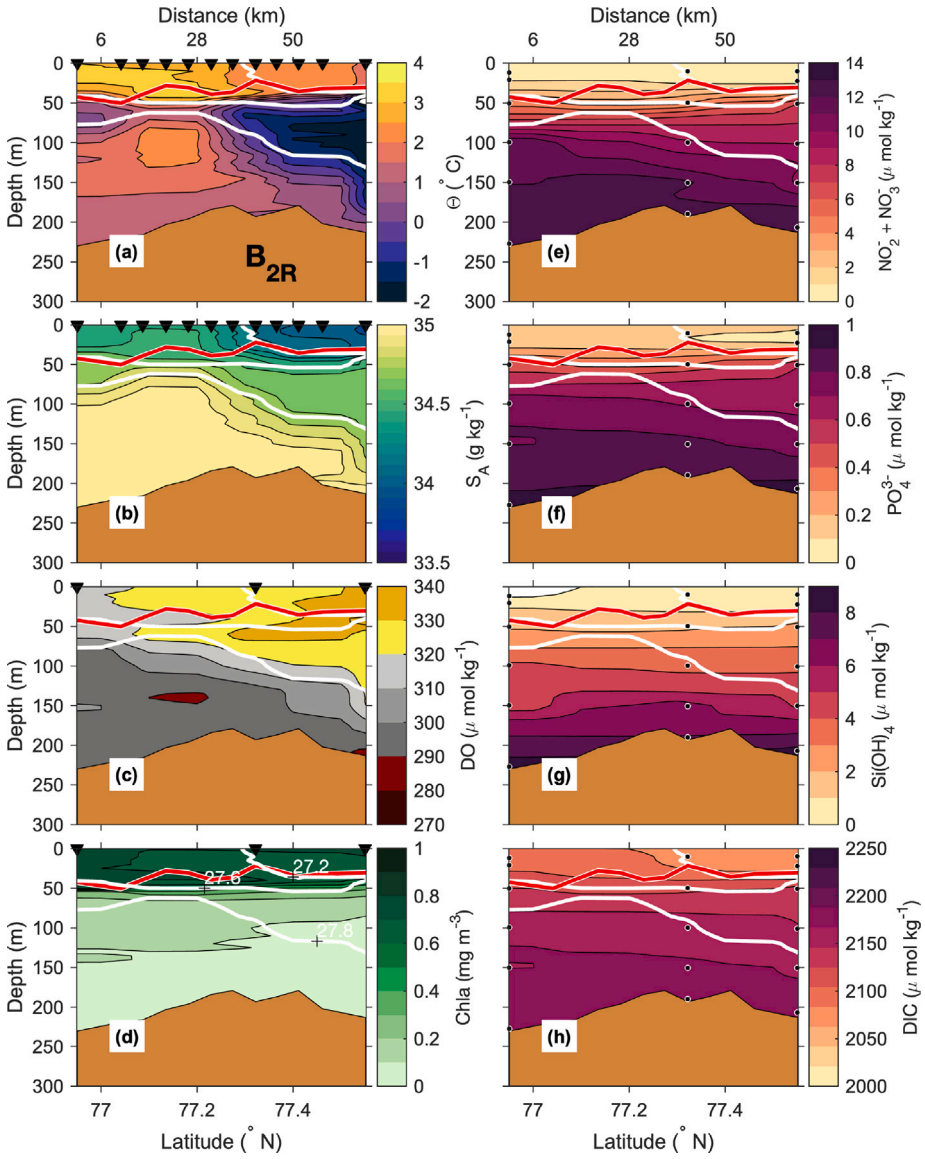

Fig. 5. Same as Fig. 4 but for the section B_{2R}: the second repeat of the B section.

silicic acid and DIC concentrations dropped (from 10 to 5 μmol kg^{-1} for the nitrate, green full and green dashed lines in Fig. 6e) within the layer from 50 to 150 m. This decrease was also observed on the south side of the sill, but not on the north/cold side where the two profiles were very similar.

On the cold side, the concentrations near the seafloor (deeper than 200 m) increased significantly from the first to the second repeat (Fig. 6), e.g., from 10 to 13 μmol kg^{-1} for the nitrate concentrations (Fig. 6a). The elevated deep values of nitrate, phosphate, silicic acid and DIC concentrations were similar to those measured on the southern side of the sill, that is Atlantic water dominated. During the second transect, Atlantic Water (Fig. 5a) was present near the bottom on the northern side of the sill. However, there was no Atlantic water on the northern side of the sill during the first repeat of the transect (Fig. 4a). The yellow profiles in Fig. 6 were collected at the station in the middle of section D that approximately aligns with section B (Fig. 1). This profile shows the presence of a strong horizontal gradient in nutrients and DIC between 50 and 100 m depth between the two sides of the front.

The presence of Atlantic Water at depth during the second repeat explains the difference in concentrations of nitrate and DIC between the two repeated transects. It also suggests that the sill is a key region and enhances exchanges between the polar domain and the Atlantic domain of the Barents Sea. This flow of Atlantic water across the sill and the potential of carrying nutrients across the sill are discussed in the next subsections.

3.2. Vertical fluxes

The dissipation rates and the vertical turbulent heat fluxes for both repeats of section B are shown in Fig. 8. The values are higher in the upper 50 m corresponding to the mixed layer, reaching 10^{-6} W kg^{-1} near the surface at 15 m depth. The average turbulence level in the upper 50 m is higher in B_{2R} compared to B_{1R}: 1.7×10^{-8} W kg^{-1} during the first repeat and 6.7×10^{-8} W kg^{-1} during the second repeat. This is caused by the increase in the wind intensity between the first and the second repeat of the section, hence more energy is provided to the upper ocean in the second repeat. Averaged heat flux over the two transects is 1 W m^{-2}, with variations up to −50 W m^{-2} (heat fluxes toward bottom) at the front in B_{1R} around 77.4°N.

Vertical turbulent fluxes of nitrate and DIC are shown in Fig. 9a and b respectively. The fluxes are directed upwards and are the largest at around 40 m depth corresponding to the approximate depth of the

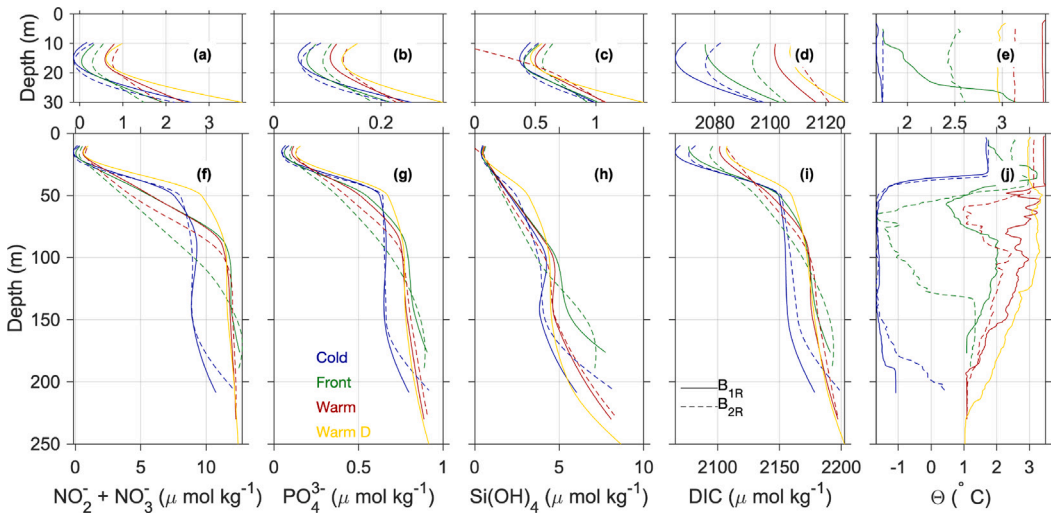

Fig. 6. Vertical profiles of (f) Nitrate (g) Phosphate (h) Silicic Acid (i) Dissolved Inorganic Carbon and (j) Conservative Temperature along section B. (a) (b) (c) (d) and (e): close up in the upper 30 m of Nitrate, Phosphate, Silicic Acid, DIC and Conservative Temperature profiles respectively. Full/Dashed line: profiles corresponding to the first/second repeat of the B section respectively. Red profiles are on the warm Atlantic water side, in the south. Blue profiles are on the cold polar side, in the north. Green profiles are on the sill, where the Polar Front is situated. The yellow profile is the middle profile in Section D, in the alignment of section B (Fig. 1).

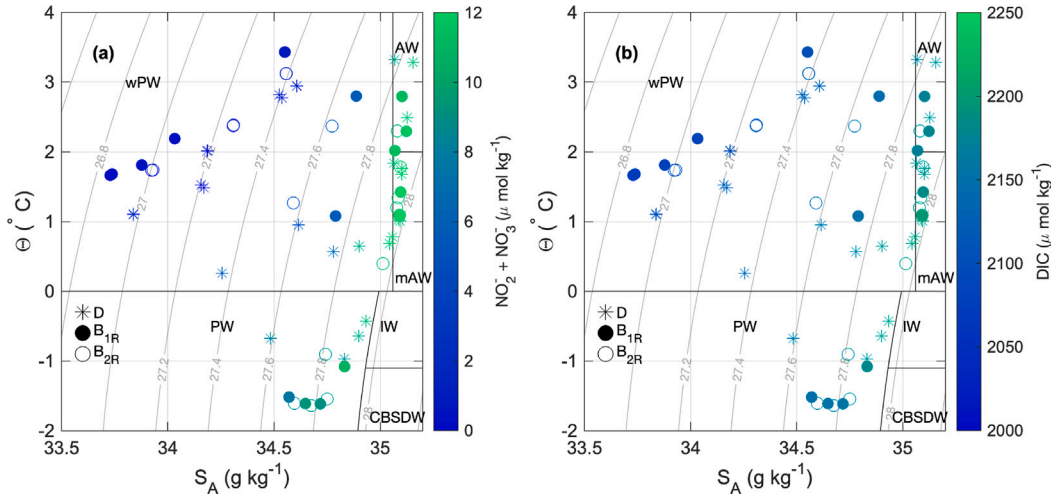

Fig. 7. Θ-S_A diagram color-coded (a) with Nitrate concentrations and (b) with DIC concentrations. Stars: section D; filled circle: section B_{1R}; empty circle: section B_{2R}; Gray lines are isolines. The water masses are indicated on the diagrams following Sundfjord et al. (2020). wPW: warm Polar Water; PW: Polar Water; AW: Atlantic Water; mAW: modified Atlantic Water; IW: Intermediate Water; CBSDW: Cold Barents Sea Deep Water.

pycnocline and nutricline. They reach 0.12 μmol m^{-2} s^{-1} for the nitrate and 0.8 μmol m^{-2} s^{-1} for DIC, both on the warm side of the front during the second repeat. The fluxes are the largest at this depth as it is a region of strong gradient in both nitrate and DIC (Eqs. 4 and 5 and Fig. 6). The fluxes vary depending on their location on the section. The sill is for both repeats the location with the least upward fluxes, 0.03 μmol m^{-2} s^{-1} for the nitrate and 0.3 μmol m^{-2} s^{-1} for the DIC during B_{2R}, as the nutricline is the least pronounced at the sill (Fig. 6). The fluxes are systematically larger in the second repeat of the transect than in the first one, and are always larger in the southern part of the transect than in the northern part. This mixing provides nitrate toward the surface where the primary production takes place (see the chlorophyll a maximum at about 10 m depth in Figs. 4d and 5d).

Vertical advective fluxes were estimated at the sill during the wind event between B_{1R} and B_{2R}. The Ekman pumping between 16 to 19 October 2020 reached 4.3×10^{-6} m s^{-1} (approximately 0.4 m day^{-1}, not shown). The difference of nitrate across the pycnocline is estimated around 10 μmol kg^{-1}, which corresponds then to a vertical advective flux of about 4.42×10^{-2} μmol m^{-2} s^{-1} across the nutricline. The vertical advective fluxes are of similar order as the vertical turbulent fluxes (Fig. 9). Hence a wind event in the Barents Sea can contribute to total (diffusive and advective) vertical fluxes of up to 0.1 μmol m^{-2} s^{-1}, by summing the contributions from advective and turbulent vertical fluxes. Fransson et al. (2017) found substantial increases of nitrate and DIC concentrations after storm events in winter in the Arctic Ocean.

3.3. Horizontal fluxes

As suggested in Fig. 5, modified Atlantic Water can be found deeper than 150 m in the northern Barents Sea (Jones et al. (2023) also show modified Atlantic Water between 100–300 m depth at P1). E. Kolås (personal communications) used data from the same cruise (October 2020) to assess the flow of Atlantic Water across the sill. They found that Atlantic water can cross the sill near the bottom, and that on average 0.3±0.2 Sv of Atlantic originating water flows from the southern side towards the northern side of the sill. In our study, we found that in the fall, the Atlantic Water carried about 2 μmol kg^{-1} more of nitrate and 15 μmol kg^{-1} more of DIC than the Polar Waters (Figs. 6e and h blue and red profiles at depth). By considering this difference, the Atlantic Water brought on average about 6.2×10^2 mol s^{-1} of nitrate

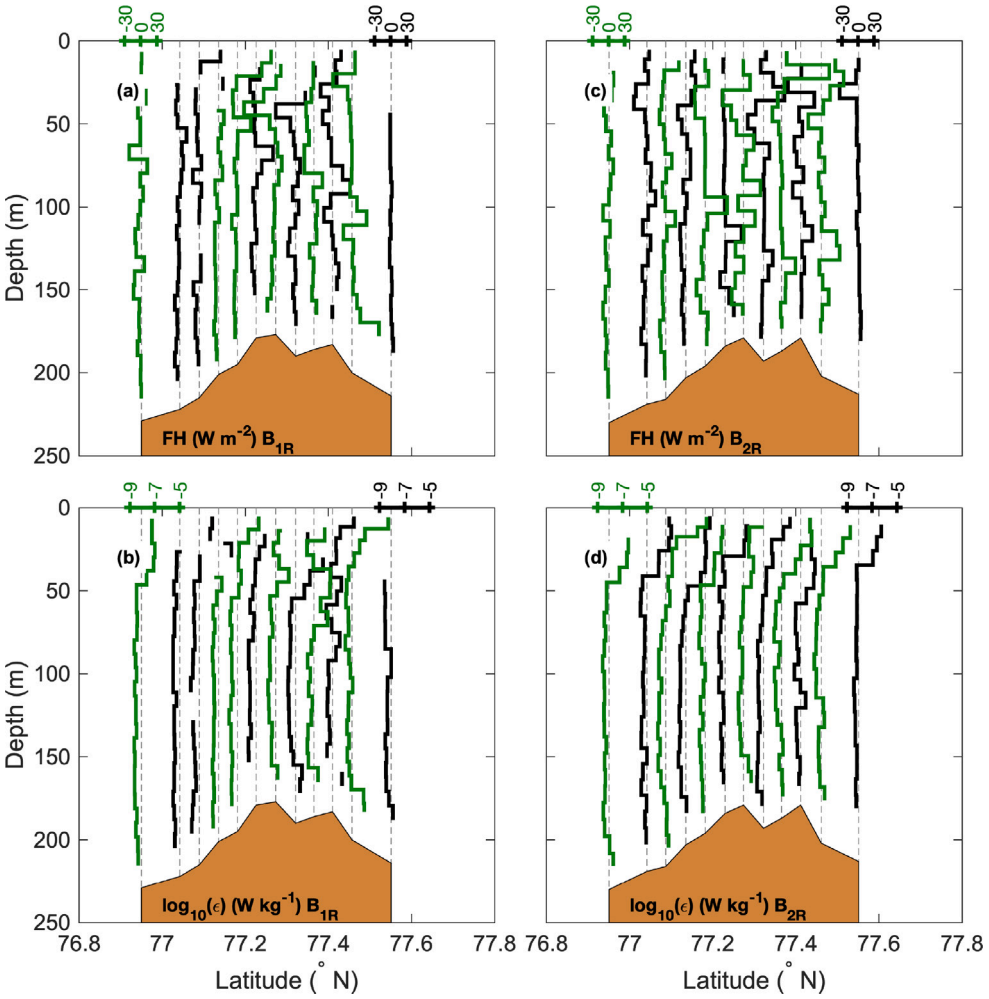

Fig. 8. Profiles of (a) and (c) vertical turbulent heat fluxes and (b) and (d) dissipation rate. Left: first repeat of the B transect. Right: second repeat of the B transect. The profiles are plotted on a topography section with respect to latitude. The dashed lines are the location of the stations. For the heat fluxes, values on the left of the dashed line are negative while they are positive on the right side. For the dissipation panels, the dashed line is the average value of dissipation over the entire section (2×10^{-9} W kg^{-1}). The reference horizontal axes for dissipation rate and vertical turbulent heat fluxes (identical for each profile) are shown in the upper part of each panel.

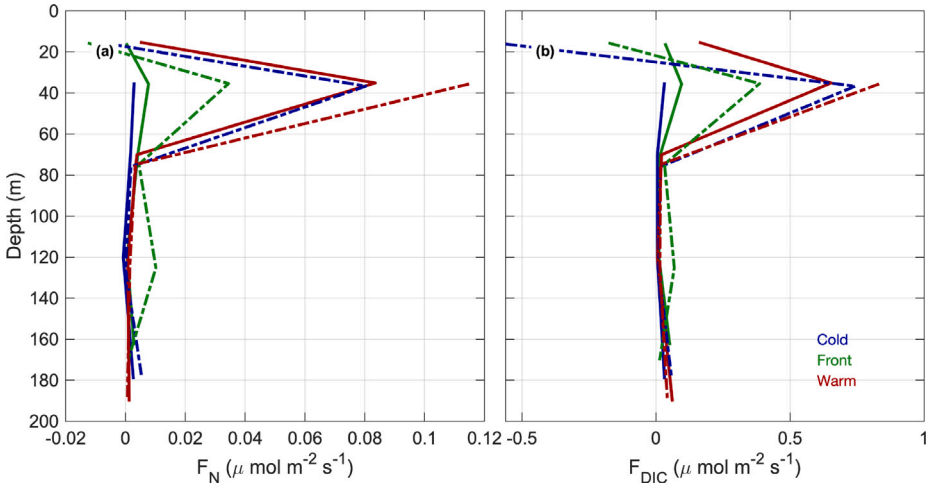

Fig. 9. (a) Vertical turbulent nitrate fluxes and b) Vertical turbulent DIC fluxes computed for the cold north side (blue profiles), sill (green profiles) and warm south side (red profiles). Full/Dashed lines: first/second repeat of the B section.

and about 4.5×10^3 mol s^{-1} of DIC into the Polar domain of the Barents Sea across the sill, for a flux of about 3.7×10^3 mol s^{-1} of nitrate across the front. This number can be compared with Torres-Valdés et al. (2013) who found that about 33.6×10^3 mol s^{-1} of nitrate

enters the Barents Sea through the Barents Sea Opening. Our estimates suggest then that about 20% of the total amount of nitrate entering the Barents Sea is transferred from the Atlantic-dominated domain to the Arctic-dominated domain of the Barents Sea.

Current velocities are however highly variable around the Polar Front. Fig. 10 shows the instantaneous advective fluxes computed at the time and location of the different casts during the two repeats of the B section and the D section (see Section 2.6 for details on the computation of the fluxes).

The horizontal advective fluxes of nutrients are larger at depth than at the surface, mainly because the nutrient concentrations are largest at depth (Fig. 4 for example). Along the D section on the shallowest part on the western side of the section, fluxes are oriented towards the south. They are the signature of branches of Modified Atlantic Water recirculating towards the south. In the deeper part of the D section, fluxes are oriented towards the north, corresponding to the main flow of Atlantic Water in the Barents Sea. During the first repeat of section B, nitrate and DIC fluxes are oriented towards the east/northeast at the sill and in the northern part of the sill. It is a direct flux of Atlantic Water and hence nutrients and DIC from the Atlantic domain to the polar domain of the Barents Sea.

Across the front, the 27.6 kg m^{-3} isopycnal in the pycnocline at about 50 m depth outcrops approximately 100 km south of the sill (Fer et al., 2021). Subduction along the sloping isopycnal offers an advective pathway of the surface water from the dense, Atlantic side of the front to the pycnocline on the cold side, across the sill (Spall, 1995). We have not quantified the frontogenesis and frontal downwelling (McWilliams, 2021); however, deeper isopycnals do not outcrop, hence we do not expect a substantial contribution to the horizontal advective fluxes below 45 m from subduction of surface-layer waters.

As the Atlantic Water at the sill is located close to the bottom, the main flux of nitrate towards the northern side of the Barents Sea is the largest on the sill at depth, about 1050 μmol m^{-2} s^{-1}. For the DIC concentration it is about 3×10^5 μmol m^{-2} s^{-1}. Compared to the previous transport estimates that are presented in the beginning of this subsection, these numbers are instantaneous and discrete estimates; they do not include any lateral integration of the nitrate and DIC fluxes over a streamtube of constant volume transport.

In contrast, the second repeat of the B section shows southwest velocities on the northern side of the sill and on the sill. The southwestward velocities stand out as anomalies compared to the other transect across the front and coincide with an anticyclonic eddy developing north of the front after 12 October and reaching its peak velocities on 19 October. The eddy is observed from both hydrographic measurements and sea level anomalies from satellite, but is not shown here as it is the topic of a different study.

The Persey current and the recirculation of Atlantic Water in the Barents Sea visible on the western side of the D section have a flux of about 700 μmol m^{-2} s^{-1} of nitrate and 3 10^5 μmol m^{-2} s^{-1} of DIC towards the south, hence out of the northern Barents Sea. E. Kolås (personal communications) estimates a southward flow of about 0.4 Sv on the western side of section D. It represents an average flux of nitrate of about 4.0×10^3 mol s^{-1} and of DIC of about 6.7×10^5 mol s^{-1}.

4. Discussion

4.1. Drivers of temporal change in the vertical distribution of inorganic nutrients and carbon

Two main temporal differences are observed between the first and the second repeat of the transect across the Polar Front, regarding nutrients and DIC concentrations: an increase of concentrations in the mixed layer and a decrease of concentration in the layer 45 to 145 m on the sill and on the warm side. The increase in the mixed layer is explained by vertical mixing due to wind.

Wind speeds were larger during the second repeat of B, inducing mixing, with larger diffusivity coefficients, hence larger upwards fluxes as shown in Section 3.2. We applied a simple 1-D diffusion model to the first repeat of the transect using a depth-variable eddy diffusivity, without any external sources to quantify the importance of the vertical diapycnal mixing in the variations between the two transects. For more details on the methodology, one can consult Fer et al. (2017). Within 3 days, vertical mixing and an increase in entrainment from below can explain a variation of 0.7 μmol kg^{-1} in the nitrate concentration in the mixed layer, which is of the same order as that which is observed in the observations (increase of about 0.5 μmol kg^{-1} at the shallowest measurement, Fig. 6a). This entrainment is most likely caused by an increase in the vertical mixing and a deepening of the mixed layer. Increased nitrate concentrations and DIC in the upper 10–20 m were observed during storm events in winter in the Nansen Basin (Fransson et al., 2017), hence it supports the results in this study.

Regarding the layer between 50 and 150 m depth, the diapycnal mixing alone cannot explain the differences in the nitrate concentrations between the first and the second repeat of the B transect (Fig. 6). Differences in concentrations mainly of nutrients at the sill and on the warm side of the section are most likely due to lateral advection. The decrease in nutrient concentrations is associated with a southward displacement of the Polar Front and of the Polar Waters that are lower in nutrients and DIC compared to the Atlantic Water (Fig. 5). Another important factor not investigated here is the tidal forcing. The sill in the Barents Sea is a region with substantial tidal forcing which contributes to the differences in the profiles at the sill.

With the expected increase of the wind forcing in the Barents Sea in the coming years (Vavrus and Alkama, 2022), one can expect an increase of the vertical fluxes of nutrients in the Barents Sea. The data were collected in 2020, during a period of positive Arctic Dipole, which contributed to slowing the sea-ice loss in the Barents Sea (Polyakov et al., 2023). A shift to the negative phase of the Arctic Dipole might accelerate Arctic sea-ice decline, leading to increased destratification of the surface layer and consequently enhancing vertical nutrient fluxes towards the surface. An increase in the flux of nutrients towards the surface (Jones et al., 2023) will drive the increase in primary production, a scenario supported by remote sensing (Lewis et al., 2020). Hence getting a better comprehension of the drivers of the nitrate fluxes in the Barents Sea under strong wind events is needed. Understanding the nitrate fluxes in both the Arctic-dominated and the Atlantic-dominated regimes of the Barents Sea is also key as the region is undergoing Atlantification (Årthun et al., 2012).

4.2. Importance of inorganic nutrient fluxes for primary production

We examined the nitrate and DIC fluxes in the autumn, when the primary production is low and the mixed layer is largely depleted in nutrients. The late autumn and winter seasons are the time when the mixed layer starts to become replenished with nutrients due to organic matter remineralization and vertical mixing, pre-conditioning the water column prior to the spring bloom (Jones et al., 2023) and mixing (Chierici et al., 2011). During a wind event, we estimated average vertical turbulent fluxes of nitrate up to 0.1 μmol m^{-2} s^{-1} and the vertical advective fluxes of about 0.04 μmol m^{-2} s^{-1} (see Section 3.2). These fluxes are of similar order as those obtained by Randelhoff et al. (2016) who reported fluxes of 0.083 μmol m^{-2} s^{-1} and 0.19 μmol m^{-2} s^{-1} under sea ice and in open water, respectively, north of Svalbard.

To generalize the response to wind events over a longer time scale, we use the ERA5 wind data from 2010 to 2022 to estimate the number of 'stormy' days in the Barents Sea from October until the end of March. We define a day 'stormy' when wind speed at 10 m height exceeds 12 m s^{-1}. On average there were 30 stormy days per winter over the last 10 years. We applied the 1-D vertical diffusion model to the nitrate profile in October assuming that the eddy diffusivity profile $K_\rho(z)$ is the same during all the stormy days. After 30 days, the nitrate value

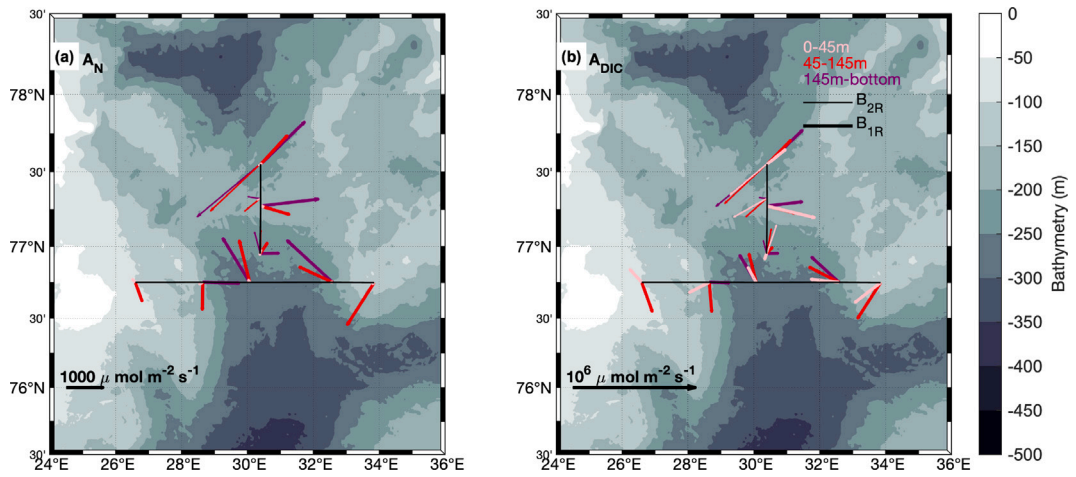

Fig. 10. Horizontal advective fluxes of (a) Nitrate (A_N) and (b) Dissolved Inorganic Carbon (A_{DIC}) during the first/second repeat of the B section (thick/thin lines respectively) and along the D section. Purple: 145 m to bottom. Red: 45 to 145 m depth. Pink: 0–45 m depth. Background is bathymetry.

in the mixed layer increased by about 2 μmol m^{-2} s^{-1}. The vertical advective fluxes during these stormy days are responsible for a similar increase, between 1.5 and 2 μmol m^{-2} s^{-1}. Hence vertical processes during stormy days can explain replenishment of nitrate in the mixed layer of about 3.5-4 μmol m^{-2} s^{-1} during the winter. Vertical fluxes (advective and turbulent) during storms are then responsible for about 1/4 of the replenishment of the mixed layer in nitrate. The rest of the replenishment can be attributed to lateral advection. This estimate is rough, as we consider a constant value for eddy diffusivity, and do not account for the presence of sea ice that might affect the estimates through, e.g., dampening wind forcing and mixing (Meyer et al., 2017).

Fluxes of nutrients are expected to evolve with the ongoing changes such as warming and sea ice decline in the Barents Sea. Koenig et al. (2023) found that less freshwater input in a future ice-free Barents Sea will have a positive impact on surface nutrient inventories by decreasing the surface stratification and will likely result in increased annual new pelagic production and harvestable marine resources from zooplankton to fish. This is consistent with a previous study that have shown a negative impact of sea ice-derived meltwater stratification on the biological carbon pump (von Appen et al., 2021).

5. Conclusion

We took advantage of concomitant measurements of turbulence and biogeochemical variables (nitrate, phosphate, silicic acid and DIC) to quantify the vertical and lateral fluxes in the Barents Sea over a 21-day period in October 2020, with implications for primary production in the following growing season. We investigated the exchanges between the Atlantic Water and the surface layer, and the exchanges across the Polar Front, between the Atlantic Water in the south and the Polar Water in the north.

We found that vertical turbulent fluxes of nitrate reached 0.12 μmol m^{-2} s^{-1} on the southern side of the front and 0.08 μmol m^{-2} s^{-1} on the northern side of the front respectively across the nutricline. Vertical turbulent fluxes of DIC were largest across the pycnocline, reaching 0.08 μmol m^{-2} s^{-1}. Vertical fluxes driven by Ekman pumping were of similar order as the vertical turbulent fluxes. We estimated that about one quarter of the replenishment in nitrate of the mixed layer in winter can be explained by the vertical advective and turbulent fluxes during 30 windy days in the Barents Sea.

Horizontal advection of nutrients and DIC occurred across the Polar Front, from the Atlantic domain to the Polar domain of the Barents Sea. Fluxes were estimated around 6×10^2 mol s^{-1} for nitrate, and about 4.5×10^3 mol s^{-1} for DIC. This represents about 20% of the fluxes of nutrient entering the Barents Sea through the Barents Sea Opening. There was also advection of nitrate and DIC towards the south and in the direction of Storfjorden.

Since conducted in autumn when the primary production is declining, this study gives an indication of the contribution and dynamics of nutrient fluxes in the Barents Sea, which are crucial for pre-conditioning the water column for primary production in the subsequent growing season.

Open research

The cruise data are available from the Norwegian Marine Data Centre: (Fer et al., 2023a,b). Bathymetric contours shown in maps are from the International Bathymetric Chart of the Arctic Ocean (IBCAO-v4) (Jakobsson et al., 2012). Wind and surface flux data are from ERA5 (Hersbach et al., 2018).

Declaration of competing interest

The authors declare that they have no known competing financial interests or personal relationships that could have appeared to influence the work reported in this paper.

Data availability

Data availability is described in the open research statement of the manuscript.

Acknowledgments

This work was supported by the Research Council of Norway through the Nansen Legacy Project, project number 276730. We thank the officers, crew and scientists of the *G.O. Sars* cruise in October 2020. We thank Eva Falck (UNIS) for water sampling and dissolved oxygen measurements for calibration of oxygen sensor data, and Christine Gawinsky (UiT) for chlorophyll a measurements. Two anonymous reviewers provided constructive suggestions that helped to improve the manuscript.

References

Årthun, M., Eldevik, T., Smedsrud, L., Skagseth, Ø., Ingvaldsen, R., 2012. Quantifying the influence of Atlantic heat on Barents Sea ice variability and retreat. J. Clim. 25 (13), 4736–4743. http://dx.doi.org/10.1175/JCLI-D-11-00466.1.

Assmy, P., Fernández-Méndez, M., Duarte, P., Meyer, A., Randelhoff, A., Mundy, C.J., Olsen, L.M., Kauko, H.M., Bailey, A., Chierici, M., et al., 2017. Leads in Arctic pack ice enable early phytoplankton blooms below snow-covered sea ice. Sci. Rep. 7 (1), 40850. http://dx.doi.org/10.1038/srep40850.

Barton, B.I., Lenn, Y.-D., Lique, C., 2018. Observed Atlantification of the Barents Sea causes the Polar Front to limit the expansion of winter sea ice. J. Phys. Oceanogr. 48 (8), 1849–1866. http://dx.doi.org/10.1175/JPO-D-18-0003.1.

Chierici, M., Fransson, A., Lansard, B., Miller, L.A., Mucci, A., Shadwick, E., Thomas, H., Tremblay, J.-E., Papakyriakou, T.N., 2011. Impact of biogeochemical processes and environmental factors on the calcium carbonate saturation state in the Circumpolar Flaw lead in the Amundsen Gulf, Arctic Ocean. J. Geophys. Res.: Oceans 116 (C9), http://dx.doi.org/10.1029/2011JC007184.

Chierici, M., Fransson, A., Wassmann, P., 2018. Arctic chemical oceanography at the edge: Focus on carbonate chemistry. In: At the edge. Vol. 343.

Dickson, A.G., Sabine, C.L., Christian, J.R., 2007. Guide to Best Practices for Ocean CO2 Measurements. North Pacific Marine Science Organization, http://dx.doi.org/10.25607/OBP-1342.

Erofeeva, S., Egbert, G., 2020. Arc5km2018: Arctic Ocean Inverse Tide Model on a 5 Kilometer Grid, 2018. Dataset. Arctic Data Center, http://dx.doi.org/10.18739/A21R6N14K.

Fer, I., 2009. Weak vertical diffusion allows maintenance of cold halocline in the central Arctic. Atmos. Oceanic Sci. Lett. 2 (3), 148–152. http://dx.doi.org/10.1080/16742834.2009.11446789.

Fer, I., Baumann, T., Elliott, F., Kolås, E.H., 2023a. Ocean microstructure measurements using an MSS profiler during the Nansen Legacy cruise, GOS2020113, October 2020. http://dx.doi.org/10.21335/NMDC-239170563.

Fer, I., Baumann, T.M., Koenig, Z., Muilwijk, M., Tippenhauer, S., 2022. Upper-Ocean Turbulence Structure and Ocean-Ice Drag Coefficient Estimates Using an Ascending Microstructure Profiler During the MOSAiC drift. J. Geophys. Res.: Oceans 127 (9), http://dx.doi.org/10.1029/2022JC018751, e2022JC018751.

Fer, I., Peterson, A.K., Randelhoff, A., Meyer, A., 2017. One-dimensional evolution of the upper water column in the Atlantic sector of the Arctic Ocean in winter. J. Geophys. Res.: Oceans 122 (3), 1665–1682. http://dx.doi.org/10.1002/2016JC012431.

Fer, I., Skogseth, R., Astad, S.S., Baumann, T., Elliott, F., Falck, E., Gawinski, C., Kolås, E.H., 2021. SS-MSC2 Process cruise/mooring service 2020: Cruise Report, no. 20, The Nansen Legacy Report Series, http://dx.doi.org/10.7557/nlrs.5798.

Fer, I., Skogseth, R., Astad, S., Baumann, T., Elliott, F., Falck, E., Gawinsky, C., Kalhagen, K., Kolås, E.H., 2023b. Ocean hydrography and current profiles from the Nansen Legacy cruise to the northern Barents Sea, GOS2020113, October 2020. http://dx.doi.org/10.21335/NMDC-1752779505.

Fransson, A., Chierici, M., Anderson, L.G., Bussmann, I., Kattner, G., Jones, E.P., Swift, J.H., 2001. The importance of shelf processes for the modification of chemical constituents in the waters of the Eurasian Arctic Ocean: Implication for carbon fluxes. Cont. Shelf Res. 21 (3), 225–242. http://dx.doi.org/10.1016/S0278-4343(00)00088-1.

Fransson, A., Chierici, M., Skjelvan, I., Olsen, A., Assmy, P., Peterson, A.K., Spreen, G., Ward, B., 2017. Effects of sea-ice and biogeochemical processes and storms on under-ice water fCO2 during the winter-spring transition in the high Arctic Ocean: Implications for sea-air CO2 fluxes. J. Geophys. Res.: Oceans 122 (7), 5566–5587. http://dx.doi.org/10.1002/2016JC012478.

Gawarkiewicz, G., Plueddemann, A.J., 1995. Topographic control of thermohaline frontal structure in the Barents Sea Polar Front on the south flank of Spitsbergen Bank. J. Geophys. Res.: Oceans 100 (C3), 4509–4524. http://dx.doi.org/10.1029/94JC02427.

Goodman, L., Levine, E.R., Lueck, R.G., 2006. On measuring the terms of the turbulent kinetic energy budget from an AUV. J. Atmos. Ocean. Technol. 23 (7), 977–990. http://dx.doi.org/10.1175/JTECH1889.1.

Graham, M., Itkin, P., Meyer, A., Sundfjord, A., Spreen, G., Smedsrud, L., Liston, G., Cheng, B., Cohen, L., Divine, D., Fer, I., Fransson, A., Gerland, S., Haapala, J., Hudson, S.R., Johansson, M., King, J., Merkouriadi, I., Peterson, A., Provost, C., Randelhoff, A., Rinke, A., Rosel, A., Sennchael, N., Walden, V., Duarte, P., Assmy, P., Steen, H., Granskog, M., 2019. Winter storms accelerate the demise of sea ice in the Atlantic Sector of the Arctic Ocean. Sci. Rep. http://dx.doi.org/10.1038/s41598-019-45574-5.

Grasshoff, P., 1983. Methods of seawater analysis. Verlag chemie. FRG 419, 61–72.

Gregg, M., D'Asaro, E., Riley, J., Kunze, E., 2018. Mixing efficiency in the ocean. Ann. Rev. Mar. Sci. 10, 443–473. http://dx.doi.org/10.1146/annurev-marine-121916-063643.

Gundersen, K., Møgster, J.S., Lien, V.S., Ershova, E., Lunde, L.F., Arnesen, H., Olsen, A.-K., 2022. Thirty Years of Nutrient Biogeochemistry in the Barents Sea and the adjoining Arctic Ocean, 1990–2019. Sci. Data 9 (1), 649. http://dx.doi.org/10.1038/s41597-022-01781-w.

Henley, S.F., Porter, M., Hobbs, L., Braun, J., Guillaume-Castel, R., Venables, E.J., Dumont, E., Cottier, F., 2020. Nitrate supply and uptake in the Atlantic Arctic sea ice zone: seasonal cycle, mechanisms and drivers. Phil. Trans. R. Soc. A 378 (2181), 20190361. http://dx.doi.org/10.1098/rsta.2019.0361.

Hersbach, H., Bell, B., Berrisford, P., Biavati, G., Horányi, A., Muñoz Sabater, J., Nicolas, J., Peubey, C., Radu, R., Rozum, I., et al., 2018. ERA5 hourly data on single levels from 1979 to present. In: Copernicus Climate Change Service (C3S) Climate Data Store, Vol. 10. CDS, ECMWF Reading, UK, http://dx.doi.org/10.24381/cds.adbb2d47.

Ingvaldsen, R.B., Assmann, K.M., Primicerio, R., Fossheim, M., Polyakov, I.V., Dolgov, A.V., 2021. Physical manifestations and ecological implications of Arctic Atlantification. Nat. Rev. Earth Environ. 2 (12), 874–889. http://dx.doi.org/10.1038/s43017-021-00228-x.

Ingvaldsen, R., Loeng, H., Asplin, L., 2002. Variability in the Atlantic inflow to the Barents Sea based on a one-year time series from moored current meters. Cont. Shelf Res. 22 (3), 505–519. http://dx.doi.org/10.1016/S0278-4343(01)00070-X.

Jakobsson, M., Mayer, L., Coakley, B., Dowdeswell, J.A., Forbes, S., Fridman, B., Hodnesdal, H., Noormets, R., Pedersen, R., Rebesco, M., Schenke, H.W., Zarayskaya, Y., Accettella, D., Armstrong, A., Anderson, R.M., Bienhoff, P., Camerlenghi, A., Church, I., Edwards, M., Gardner, J.V., Hall, J.K., Hell, B., Hestvik, O., Kristoffersen, Y., Marcussen, C., Mohammad, R., Mosher, D., Nghiem, S.V., Pedrosa, M.T., Travaglini, P.G., Weatherall, P., 2012. The International Bathymetric Chart of the Arctic Ocean (IBCAO) version 3.0. Geophys. Res. Lett. 39, http://dx.doi.org/10.1029/2012gl052219.

Johnson, K.M., Körtzinger, A., Mintrop, L., Duinker, J.C., Wallace, D.W., 1999. Coulometric total carbon dioxide analysis for marine studies: measurement and internal consistency of underway TCO2 concentrations. Mar. Chem. 67 (1–2), 123–144. http://dx.doi.org/10.1016/S0304-4203(99)00055-9.

Jones, E.M., Chierici, M., Fransson, A., Assmann, K.M., Renner, A.H., Hodal Lødemel, H., 2023. Inorganic carbon and nutrient dynamics in the marginal ice zone of the Barents Sea: Seasonality and implications for ocean acidification. Progr. Oceanogr 219, 103131. http://dx.doi.org/10.1016/j.pocean.2023.103131.

Jones, E.M., Chierici, M., Menze, S., Fransson, A., Ingvaldsen, R.B., Lødemel, H.H., 2021. Ocean acidification state variability of the Atlantic Arctic Ocean around northern Svalbard. Prog. Oceanogr. 199, 102708. http://dx.doi.org/10.1016/j.pocean.2021.102708.

Koenig, Z., Muilwijk, M., Sandven, H., Lundesgaard, Ø., Assmy, P., Lind, S., Assmann, K., Chierici, M., Fransson, A., Gerland, S., Jones, E., Renner, A., Granskog, M., 2023. From Winter to Late Summer in the Northwestern Barents Sea: Sea Ice and Upper Ocean Evolution and Impacts on Nutrient and Phytoplankton Dynamics. Progr. Oceanogr.

Lewis, K., Van Dijken, G., Arrigo, K.R., 2020. Changes in phytoplankton concentration now drive increased Arctic Ocean primary production. Science 369 (6500), 198–202. http://dx.doi.org/10.1126/science.aay8380.

Li, S., McClimans, T.A., 1998. The effects of winds over a barotropic retrograde slope current. Cont. Shelf Res. 18 (5), 457–485. http://dx.doi.org/10.1016/S0278-4343(97)00077-0.

Lind, S., Ingvaldsen, R.B., Furevik, T., 2018. Arctic warming hotspot in the northern Barents Sea linked to declining sea-ice import. Nat. Clim. Change 8 (7), 634–639. http://dx.doi.org/10.1038/s41558-018-0205-y.

Loeng, H., 1991. Features of the physical oceanographic conditions of the Barents Sea. Polar Res. 10 (1), 5–18. http://dx.doi.org/10.3402/polar.v10i1.6723.

Lueck, R.G., 2022. The statistics of oceanic turbulence measurements. Part I: Shear variance and dissipation rates. J. Atmos. Ocean. Technol. 39 (9), 1259–1271. http://dx.doi.org/10.1175/JTECH-D-21-0051.1.

McDougall, J., Barker, P., 2011. Getting started with TEOS-10 and the Gibbs Seawater (GSW) oceanographic toolbox, 28pp., SCOR/IAPSO WG127, ISBN 978-0-646-55621-5.

McWilliams, J.C., 2021. Oceanic frontogenesis. Ann. Rev. Mar. Sci. 13, 227–253. http://dx.doi.org/10.1146/annurev-marine-032320-120725.

Meyer, A., Fer, I., Sundfjord, A., Peterson, A.K., 2017. Mixing rates and vertical heat fluxes north of Svalbard from Arctic winter to spring. J. Geophys. Res. 122 (6), 4569–4586. http://dx.doi.org/10.1002/2016JC012441.

Onarheim, I.H., Eldevik, T., Smedsrud, L.H., Stroeve, J.C., 2018. Seasonal and regional manifestation of Arctic sea ice loss. J. Clim. 31 (12), 4917–4932. http://dx.doi.org/10.1175/JCLI-D-17-0427.1.

Osborn, T.R., 1980. Estimates of the local rate of vertical diffusion from dissipation measurements. J. Phys. Oceanogr. 10 (1), 83–89. http://dx.doi.org/10.1175/1520-0485(1980)010<0083:EOTLRO>2.0.CO;2.

Oziel, L., Sirven, J., Gascard, J.-C., 2016. The Barents Sea frontal zones and water masses variability (1980–2011). Ocean Sci. 12 (1), 169–184. http://dx.doi.org/10.5194/os-12-169-2016.

Pickart, R.S., Smethie, Jr., W.M., 1998. Temporal evolution of the deep western boundary current where it enters the sub-tropical domain. Deep Sea Res. Part I: Oceanogr. Res. Pap. 45 (7), 1053–1083. http://dx.doi.org/10.1016/s0967-0637(97)00084-8.

Polyakov, I.V., Ingvaldsen, R.B., Pnyushkov, A.V., Bhatt, U.S., Francis, J.A., Janout, M., Kwok, R., Skagseth, Ø., 2023. Fluctuating Atlantic inflows modulate Arctic atlantification. Science 381 (6661), 972–979. http://dx.doi.org/10.1126/science.adh5158.

Polyakov, I.V., Pnyushkov, A.V., Alkire, M.B., Ashik, I.M., Baumann, T.M., Carmack, E.C., Goszczko, I., Guthrie, J., Ivanov, V.V., Kanzow, T., Krishfield, R., Kwok, R., Sundfjord, A., Morison, J., Rember, R., Yulin, A., 2017. Greater role for Atlantic inflows on sea-ice loss in the Eurasian Basin of the Arctic Ocean. Science http://dx.doi.org/10.1126/science.aai8204.

Prandke, H., Stips, A., 1998. Test measurements with an operational microstructure-turbulence profiler: Detection limit of dissipation rates. Aquatic Sci. 60 (3), 191–209. http://dx.doi.org/10.1007/s000270050036.

Randelhoff, A., Fer, I., Sundfjord, A., Tremblay, J.-É., Reigstad, M., 2016. Vertical fluxes of nitrate in the seasonal nitracline of the Atlantic sector of the Arctic Ocean. J. Geophys. Res.: Oceans 121 (7), 5282–5295. http://dx.doi.org/10.1002/2016JC011779.

Reigstad, M., Wassmann, P., Riser, C.W., Øygarden, S., Rey, F., 2002. Variations in hydrography, nutrients and chlorophyll a in the marginal ice-zone and the central Barents Sea. J. Mar. Syst. 38 (1–2), 9–29. http://dx.doi.org/10.1016/S0924-7963(02)00167-7.

Schauer, U., Loeng, H., Rudels, B., Ozhigin, V.K., Dieck, W., 2002. Atlantic water flow through the Barents and Kara seas. Deep Sea Res. Part I: Oceanogr. Res. Pap. 49 (12), 2281–2298. http://dx.doi.org/10.1016/S0967-0637(02)00125-5.

Skagseth, Ø., Eldevik, T., Årthun, M., Asbjørnsen, H., Lien, V.S., Smedsrud, L.H., 2020. Reduced efficiency of the Barents Sea cooling machine. Nature Clim. Change 10 (7), 661–666. http://dx.doi.org/10.1038/s41558-020-0772-6.

Smedsrud, L.H., Esau, I., Ingvaldsen, R.B., Eldevik, T., Haugan, P.M., Li, C., Lien, V.S., Olsen, A., Omar, A.M., Otterå, O.H., Risebrobakken, B., Sandø, A.B., Semenov, V.A., Sorokina, S.A., 2013. The role of the barents sea in the arctic climate system. Rev. Geophys. 51 (3), 415–449. http://dx.doi.org/10.1002/rog.20017.

Smith, W.H.F., Wessel, P., 1990. Gridding with continuous curvature splines in tension. Geophysics 55 (3), 293. http://dx.doi.org/10.1190/1.1442837.

Spall, M.A., 1995. Frontogenesis, subduction, and cross-front exchange at upper ocean fronts. J. Geophys. Res.: Oceans 100 (C2), 2543–2557. http://dx.doi.org/10.1029/94JC02860.

Sundfjord, A., Assmann, K.M., Lundesgaard, Ø., Renner, A.H., Lind, S., Ingvaldsen, R.B., 2020. Suggested Water Mass Definitions for the Central and Northern Barents Sea, and the Adjacent Nansen Basin. no. 8. In: The Nansen Legacy Report Series, http://dx.doi.org/10.7557/nlrs.5707.

The Nansen Legacy, 2021. Sampling protocols: Version 7, Vol. 17/2021. In: The Nansen Legacy Report Series.

Thurnherr, A.M., 2010. A practical assessment of the errors associated with full-depth LADCP profiles obtained using Teledyne RDI workhorse acoustic Doppler current profilers. J. Atmos. Ocean. Technol. 27 (7), 1215–1227. http://dx.doi.org/10.1175/2010JTECHO708.1.

Torres-Valdés, S., Tsubouchi, T., Bacon, S., Naveira-Garabato, A.C., Sanders, R., McLaughlin, F.A., Petrie, B., Kattner, G., Azetsu-Scott, K., Whitledge, T.E., 2013. Export of nutrients from the Arctic Ocean. J. Geophys. Res.: Oceans 118 (4), 1625–1644. http://dx.doi.org/10.1002/jgrc.20063.

Våge, S., Basedow, S., Tande, K., Zhou, M., 2014. Physical structure of the Barents Sea Polar Front near Storbanken in august 2007. J. Mar. Syst. 130, 256–262. http://dx.doi.org/10.1016/j.jmarsys.2011.11.019.

Vavrus, S.J., Alkama, R., 2022. Future trends of arctic surface wind speeds and their relationship with sea ice in CMIP5 climate model simulations. Clim. Dynam. 59 (5–6), 1833–1848. http://dx.doi.org/10.1007/s00382-021-06071-6.

Visbeck, M., 2002. Deep velocity profiling using lowered acoustic Doppler current profilers: Bottom track and inverse solutions. J. Atmos. Ocean. Technol. 19 (5), 794–807. http://dx.doi.org/10.1175/1520-0426(2002)019<0794:DVPULA>2.0.CO;2.

von Appen, W.-J., Waite, A.M., Bergmann, M., Bienhold, C., Boebel, O., Bracher, A., Cisewski, B., Hagemann, J., Hoppema, M., Iversen, M.H., et al., 2021. Sea-ice derived meltwater stratification slows the biological carbon pump: Results from continuous observations. Nature Commun. 12 (1), 7309. http://dx.doi.org/10.1038/s41467-021-26943-z.